# Theoretical and experimental investigation of acoustic streaming in a porous material

Pietro Poesio, Gijs Ooms, and Arthur Schraven
*J. M. Burgerscentrum, Delft University of Technology, Laboratory for Aero- and Hydrodynamics, Leeghwaterstraat 21, 2628 CB Delft, The Netherlands*

Fred van der Bas
*Shell International Exploration and Production, Technology Application and Research, P.O. Box 60, 2280 AB Rijswijk, The Netherlands*
(Received 15 October 2001; published 30 July 2002)

An experimental and theoretical investigation of the influence of high-frequency acoustic waves on the flow of a liquid through a porous material has been made. Particular attention was paid to the phenomenon of acoustic streaming of the liquid in the porous material due to the damping of the acoustic waves. The experiments were performed on Berea sandstone cores. Two acoustic horns were used with frequencies of 20 and 40 kHz, and with maximum power output of 2 and 0.7 kW, respectively. A high external pressure was applied in order to avoid cavitation. A microphone was used to measure the damping of the waves in the porous material and also temperature and pressure measurements in the flowing liquid inside the cores were carried out. To model the acoustic streaming effect Darcy's law was extended with a source term representing the momentum transfer from the acoustic waves to the liquid. The model predictions for the pressure distribution inside the core under acoustic streaming conditions are in reasonable agreement with the experimental data.

DOI: 10.1103/PhysRevE.66.016309 PACS number(s): 43.25.+y

## I. INTRODUCTION

In earlier publications (see Refs. [1] and [2]) we reported about an experimental and theoretical investigation of the influence of high-frequency acoustic waves on the flow of a liquid through a porous material. The experiments were performed on Berea sandstone cores. The reason for this type of sandstone is that next to a fundamental study we are also interested in an application of high-frequency acoustic waves to clean the near well bore region of an oil reservoir, and Berea sandstones are representative of the type of porous material in an oil reservoir. Two acoustic horns were used with frequencies of 20 and 40 kHz, and with maximum power output of 2 and 0.7 kW, respectively. A high external pressure was applied in order to avoid cavitation. The acoustic waves were found to produce a significant effect on the pressure gradient at constant liquid flow rate through the core samples: during the application of acoustic waves the pressure gradient inside the core decreased. This effect turned out to be due to the decrease of the liquid viscosity caused by an increase in liquid temperature as a result of the acoustic energy dissipation inside the porous material. Also a theoretical model was developed to calculate the dissipation effect on the viscosity and on the pressure gradient. The model predictions were in reasonable agreement with the experimental data.

In this paper, we will report about another effect of high-frequency acoustic waves on the flow of a liquid through a porous material; viz. the streaming effect due to the damping of the acoustic waves. A traveling acoustic wave in a liquid induces a net steady flow in the direction of its propagation. This effect can only occur when the wave is being attenuated. The phenomenon is called acoustic streaming and is described in detail in the book by Lighthill (see Ref. [3]). From a physical point of view acoustic streaming is due to a transfer of momentum from the traveling acoustic wave to the liquid. A planar, traveling wave with intensity $I$ has momentum

$$M = \frac{I}{c^2}, \tag{1}$$

where $c$ is the velocity of sound in the medium in which the wave propagates. There is a relation between energy and momentum. While energy is dissipated into heat in the liquid, momentum is passed on to the liquid. This generates a net steady flow away from the sound source. So even without a pressure drop over a core of porous material before the acoustic source is switched on, the liquid inside the core will start flowing after the source is switched on due to this momentum transfer. As the damping of high-frequency acoustic waves in a liquid inside a porous material is strong, also a strong and measurable acoustic streaming effect may be expected in such a material. To investigate this effect we have carried out streaming experiments in the experimental setup mentioned above. During these experiments there was no pressure drop over the core before the acoustic horn was switched on. After the horn was put into action, the liquid started to flow. Because of the liquid flow and the momentum transfer from the acoustic wave a pressure profile developed inside the core as a function of time. This pressure profile development was measured. Also a theoretical model was developed to predict the streaming effect on the development of the pressure distribution inside the core. In this publication we report about this experimental and theoretical investigation.

## II. DESCRIPTION OF THE EXPERIMENTS

The experiments were carried out in the setup shown in Fig. 1. The cores that were used for the experiments were cylindrically shaped Berea sandstone samples. The length of

 

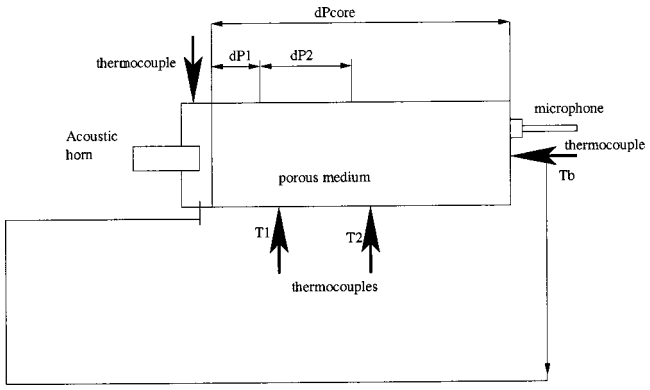


FIG. 1. Experimental setup.

the cores was 20 cm and the diameter 7.62 cm. The porosity was about 0.25. The initial permeability was 100–300 mdarcy for all samples. During an experiment a core was placed in a rubber sleeve to keep it fixed during the experiment. It was then placed in a steel vessel in which down-hole reservoir conditions were simulated (up to 150 bars and 100 °C). An acoustic horn was placed at one end of the core (see Fig. 1). The high pressure in the vessel made it possible to avoid cavitation (for pressures lower than 100 bars the influence of cavitation becomes noticeable). The space between the vessel and sleeve, which was filled with water, was pressurized to 180 bars to make the rubber sleeve completely seal off.

There were four pressure measurements, two along the core (at 2.54 and 10.70 cm) and two at both ends of the core (see Fig. 1). $dP_1$ is the pressure drop over the first part of the core sample, $dP_2$ is the pressure drop over the middle part, and $dP_c$ is the total pressure drop over the core. The pressure drop over the third part $dP_3$ can be calculated in the following way: $dP_3 = dP_c - (dP_1 + dP_2)$. To measure the temperature at two locations in the core ($T_1$ and $T_2$) we installed two thermocouples at the sidewall of the porous medium, through the rubber sleeve (see Fig. 1). Also the temperature in front and at the back ($T_b$) of the core could be measured. The data were sent to a digital data recorder and processed on a computer.

The ultrasonic equipment consisted of (1) a converter, which converts electricity into mechanical vibrations of a piezoelectric element; (2) an amplifier, which is used to set the amplitude of the vibrations; and (3) an ultrasonic horn, which concentrates the mechanical vibrations onto the front side of the core sample. Two acoustic horns were applied: a Branson Module PGA 220 (a 20 kHz horn with maximum power output of 2 kW) and a Branson Module PGA 470 (a 40 kHz horn with maximum power output of 0.7 kW). The power output could be selected as a percentage of the maximum.

A microphone was placed at the end side of the core. It was used to measure the amplitude of the acoustic signal after passage through the core. In this way the damping of the signal was determined during the experiments.

A new core was used for each new series of experiments. Before performing experiments, the following steps were taken.

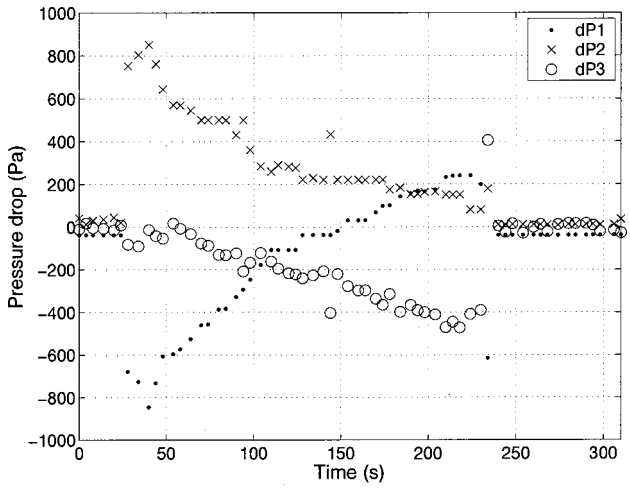


FIG. 2. An example of the three pressure drops evolution during the sonification time.

(1) The core was flushed with $CO_2$ to expel all the air in the porous material. The gas flow was kept on for several minutes.

(2) After the gas flow was stopped, a constant flow rate of brine was started. The high pressure ensured that all the $CO_2$ dissolved into the brine. Brine instead of water was used in order to avoid the generation of fine clay particles inside the core sample by the swelling of clay (for more details see Khilar and Fogler [4]).

(3) The flow rate was increased up to the maximum value that the pump could deliver to detach and remove possible fines that were present in the core sample.

During a streaming experiment we set the initial temperature in the cell, the pore pressure ($p_{\mathrm{pore}}$), and the confining pressure ($p_{\mathrm{conf}}$). The two ends of the core were connected via a pipe (see Fig. 1), so no external pressure drop over the core was applied. This means that the pressure distribution inside the core was uniform before the acoustic horn was switched on. After the acoustic horn was switched on we measured the pressure profile inside the core as a function of time by measuring the pressure development at the front and back side of the core and at the two points inside the core. The development of this pressure profile is due to the acoustic streaming phenomenon: the transfer of momentum from the acoustic wave to the liquid. Also the temperatures at the two points inside the core ($T_1$ and $T_2$) and at the back ($T_b$) were measured as functions of time. The temperature change is due to the dissipation of the acoustic wave. Some typical results that we got during these experiments are given in Fig. 2 (where the pressure drop evolution over the three parts of the core is shown) and in Fig. 3 (where the temperature evolution of $T_1$, $T_2$, and $T_b$ is shown). Calculations show that the temperature profile in a cross section of the core is almost uniform. In Fig. 2 two discontinuities are present in the pressure drop profile: one at 25 sec which corresponds to the switching on of the horn, the second at 230 sec which corresponds to the switching off. Further discussion of the results will be given in the section on experimental results. During the experiments the temperature at the back side of the core sample remained nearly constant (see Fig. 3). The

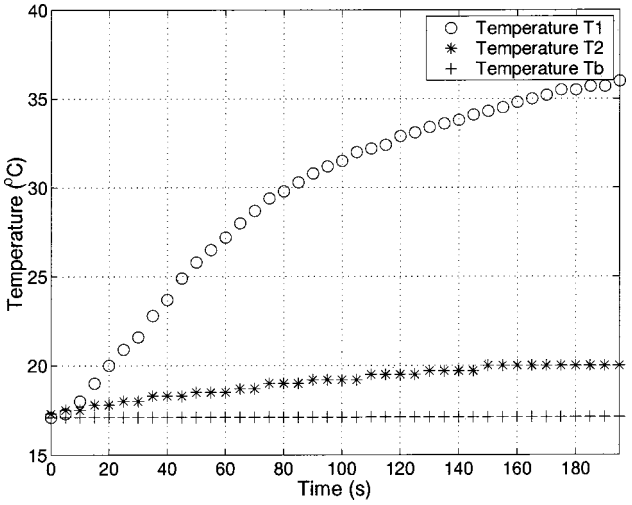


FIG. 3. An example of the temperature evolution during the sonification time.

reason is that the fast wave has almost completely dissipated its energy inside the core before it reaches the end of the core sample.

### III. THEORETICAL MODEL

The influence of the acoustic wave on the liquid flow is modeled via a source term in the momentum equation and in the energy equation. The source term in the momentum equation represents the transfer of momentum from the wave to the liquid, and the source term in the energy equation represents the dissipation of acoustic energy into heat. The flow is assumed to be incompressible. Moreover, the distribution of the pressure and velocity in a cross section of the core is assumed to be uniform. So the model equations are one dimensional with $x$ as the axial coordinate.

The continuity equation can then be written as

$$\frac{\partial v}{\partial x}=0, \tag{2}$$

where $v$ is the superficial velocity of the liquid.

For the momentum equation we use the Darcy equation extended with a time-dependent term and with a source term representing the momentum transfer. For the source term we assume, only a fraction (equal to the porosity) of the acoustic momentum is given to the liquid. The remaining part goes to the solid. In this way, the momentum equation is given by

$$\frac{\rho_f}{\phi}\frac{\partial v}{\partial t}=-\frac{\partial p}{\partial x}-\frac{\mu(T)}{K}v+S_{\mathrm{mom}}, \tag{3}$$

in which $\rho_f$ is the fluid density, $p$ is the pressure, $\phi$ is the porosity, and $K$ is the permeability. $\mu(T)$ is the viscosity, which is dependent on temperature $T$. This temperature dependence has been taken from the book by Zaytsevan and Aseyev [5]. $S_{\mathrm{mom}}$ is the rate of momentum transfer from the acoustic waves to the liquid. It can be written as

$$S_{\mathrm{mom}}=c_{\mathrm{fast}}\frac{\partial}{\partial x}(M^{\mathrm{fast}})+c_{\mathrm{slow}}\frac{\partial}{\partial x}(M^{\mathrm{slow}}), \tag{4}$$

where $M^{\mathrm{fast}}$ and $M^{\mathrm{slow}}$ are the momentum of the fast and slow wave, respectively. $c_{\mathrm{fast}}$ and $c_{\mathrm{slow}}$ are the velocities of the fast and slow wave. For the sake of completeness, more details on sound wave propagation through porous media can be found in Appendix A, where we present a brief review of the Biot's theory (see also the original paper by Biot [6] for more details).

The momenta of the fast wave and slow wave $M^{\mathrm{fast}}$ and $M^{\mathrm{slow}}$ (and therefore also $S_{\mathrm{mom}}$) are functions of the axial distance $x$ due to the dissipation of the acoustic wave. For the calculation of $M^{\mathrm{fast}}$ and $M^{\mathrm{slow}}$ we used Eq. (1). This means that the acoustic intensity $I$ as function of $x$ has to be known. Due to the damping of the wave $I$ can be written as

$$I=I_{\mathrm{fast},0}e^{-2\alpha_{\mathrm{fast}}x}+I_{\mathrm{slow},0}e^{-2\alpha_{\mathrm{slow}}x}, \tag{5}$$

where $I_{\mathrm{fast},0}$ and $I_{\mathrm{slow},0}$ are the initial values (at the front end of the core) of the intensities of the fast wave and slow wave, which are transmitted in the porous material as a result of the incident acoustic wave at the front end of the core caused by the acoustic horn. There is no transmitted shear wave as the incident acoustic wave is perpendicular to the porous material surface at the front end. The intensity of the incident acoustic wave has been measured. To calculate the initial values of the intensity of the fast and the slow waves from the incident wave we used a calculation procedure proposed by Wu Xue, and Adler [7]. In Appendix B this calculation procedure is explained. As is well known, there is a strong damping of the transmitted fast wave and a very strong damping of the transmitted slow wave. These damping coefficients are given by $\alpha_{\mathrm{fast}}$ and $\alpha_{\mathrm{slow}}$. ($\alpha_{\mathrm{fast}}$ is also dependent on the temperature $T$.) The determination of the damping coefficients will be discussed later.

For the determination of $\mu(T)$ and $\alpha_{\mathrm{fast}}(T)$ we need the temperature distribution inside the core. To that purpose we solve the temperature equation

$$(\phi\rho_f c_f+(1-\phi)\rho_p c_p)\frac{\partial T}{\partial t}+\rho_f c_f v\frac{\partial T}{\partial x}=\lambda\frac{\partial^2 T}{\partial x^2}+S_{\mathrm{therm}}, \tag{6}$$

in which $c_f$ is the specific heat for the liquid, $c_p$ is the specific heat for the solid, $\rho_p$ is the solid density, $\lambda$ is the thermal conductivity of saturated rock, and $S_{\mathrm{therm}}$ is the source term due to the acoustic energy dissipation. For the thermal conductivity of saturated sandstone we used the results published by Khan and Fatt [8]. They measured the thermal conductivity for a temperature up to 80 °C and a pressure up to 125 bars. We took the heat conductivity into account, as we expected that at low velocities the heat transfer due to conduction can be important. In Eq. (6), we did not include a term representing the heat transfer from the core sample via

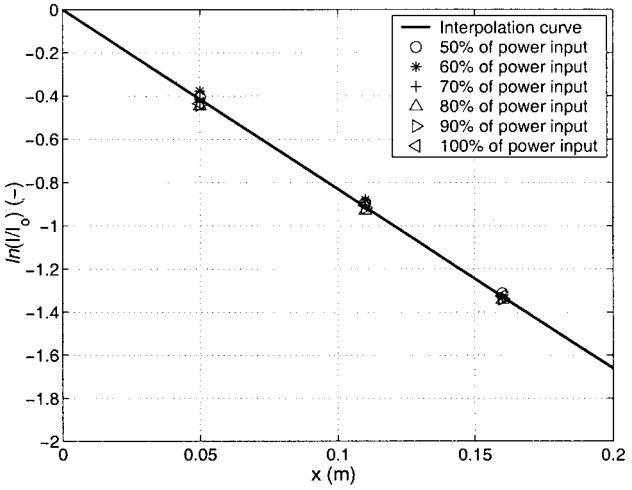


FIG. 4. Output signal as a function of core length. Symbols refer to the percentage of the power input. The Berea sandstone core is saturated with 2% KCl brine. Frequency 40 kHz, permeability 140 mdarcy, $T=20\,^{\circ}\mathrm{C}$, $p_{\mathrm{pore}}=120$ bars, and $p_{\mathrm{conf}}=185$ bars.

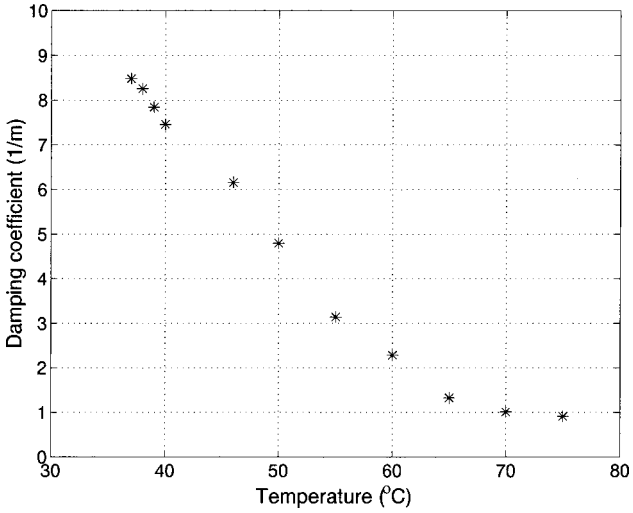


FIG. 5. Damping coefficient as function of temperature. The Berea sandstone core is saturated with 2% KCl brine. Frequency 40 kHz, permeability 140 mdarcy, $p_{\mathrm{pore}}=120$ bars, and $p_{\mathrm{conf}}=185$ bars.

the sidewall and the rubber sleeve to the water in the surrounding vessel. However, the heat conductivity of the rubber sleeve is very small and the heat loss to the water is (according to our calculation) therefore negligible compared to the convective heat transfer. The source term can be written as

$$S_{\mathrm{therm}}=\frac{\partial}{\partial x}[I_0^{\mathrm{fast}}(1-e^{2\alpha_{\mathrm{fast}}(T)x})+I_0^{\mathrm{slow}}(1-e^{-2\alpha_{\mathrm{slow}}x})]. \tag{7}$$

The following boundary conditions are applied.

(1) The flow resistance of the connecting pipe between the front side and the back side of the core is very low and, therefore, the pressures at the two sides were chosen to be equal.

(2) The temperature at the front and at back side are known functions of time: these temperatures were measured with the thermocouples placed in front and at the back of the core.

A finite difference code was written to solve the equations discussed in this section.

## IV. MEASUREMENT OF DAMPING COEFFICIENT

As mentioned, the incident acoustic wave is split in the porous material into a slow wave and a fast wave. The damping of the slow wave is very strong and is known according to Biot's theory. In Appendix A a brief review of Biot's theory and the calculation of damping coefficient are given. However, the damping of the fast wave is much more difficult to predict. Biot's theory [6] predicts a damping coefficient for the fast wave which is too low for many materials. To the best of our knowledge, no models are available that can reliably predict the damping coefficient for the fast wave. This is the reason why we decided to determine this damping coefficient for our cores experimentally. In order to measure the attenuation we used cores of different lengths and measured the damping as a function of the core length with the aid of the microphone. Each set of points could be interpolated by means of an exponential curve. In this way, the damping coefficient was determined. Six different power outputs of the acoustic horn were used. For each power output, we measured as mentioned the damping coefficient on cores of three different lengths, viz. 5, 11, and 16 cm. As the microphone was fixed at a distance of 20 cm in the experimental setup, we extended, for each core length, the core with an additional part made of a plastic material (Peek) in such a way that the total core was always 20 cm. The acoustic damping in the Peek is negligible. We measured the acoustic intensity at the end of the total core length. The results are presented in Fig. 4, where we have plotted, in a logarithmic scale, the ratio between the intensity of the attenuated wave and the input intensity as function of the position inside the core. For cores with a length of 16 cm the damping of the acoustic wave is almost complete at the back side of the core. So the intensity of the wave reflected at the back is very small and can be therefore neglected. According to our measurements this is still true for shorter core samples with a length of 11 cm. However, for the shortest core samples with a length of 5 cm the damping of the acoustic wave is not complete and therefore the intensity of the reflected wave is significant. We have not compensated for this effect by including the reflection of the wave at the back side. In our opinion this is the cause for the (rather small) scatter of our measured points a $x=5$ cm in Fig. 4. As can be seen from Fig. 4 this scatter is no longer present at $x=11$ and at $x=16$ cm, as explained above.

The damping coefficient depends, for instance, on the viscosity of the liquid. As the viscosity is temperature dependent, also the damping coefficient is dependent on the temperature. Therefore the measurement of the damping coefficient was carried out at different temperatures. In Fig. 5 we show the result. The damping coefficient decreases quickly with increasing temperature.

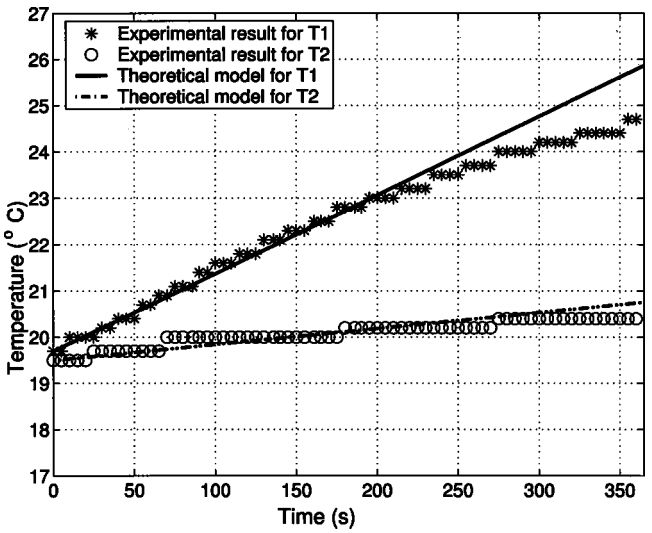


FIG. 6. Temperature evolution according to theory and experimental data for $T_1$ and $T_2$. The Berea sandstone core is saturated with 2% KCl brine. Frequency 40 kHz, permeability 140 mdarcy, $p_{\text{pore}}=120$ bars, $p_{\text{conf}}=185$ bars, and power input 184 W.

## V. COMPARISON BETWEEN EXPERIMENTAL DATA AND THEORETICAL PREDICTIONS

Two series of experiments have been carried out: one using the 20 kHz horn and one using 40 kHz horn. The results are summarized below.

### A. Experiments with 40 kHz horn

It turned out that the 40 kHz horn had a too low power output (max. 0.7 kW) to cause measurable changes in the pressure distribution inside the core. However, there was a measurable influence on the temperature distribution. A typical result is shown in Fig. 6. As can be seen the agreement between experimental data and model predictions is reasonably good.

### B. Experiments with 20 kHz horn

The power output (max. 2 kW) of the 20 kHz horn is sufficiently large to cause a measurable effect on the pressure distribution inside the core due to acoustic streaming. An example of the comparison between model predictions and experimental data is given in Figs. 7–13. As can be seen the agreement is certainly not perfect. However, the order of magnitude of the pressure distribution inside the core due to streaming and also its development as function of time is very reasonable. From a comparison of the results shown in Figs. 7–13, the strong relation between the intensity of the sound wave and the induced pressure and temperature changes can be seen. For the cases of minimum and maximum power output we also show in Figs. 7(a) and 13(a) the measured and calculated temperature distribution inside the core. As can be seen, the agreement is rather good.

At the front part of the core there is a strong pressure buildup. This is due to the momentum transfer from the acoustic wave to the liquid. According to Eq. (3) this momentum transfer is used for the pressure buildup, but also for overcoming the viscous friction of the liquid flow and for the (negligible) inertia increase of the flowing liquid. The experiments show a pressure increase at the end side of the core. This is necessary for overcoming the viscous friction of the liquid flow in the connecting pipe between the end side and the front side of the core. This effect is not incorporated in the model, as we assumed the friction of the connecting pipe to be negligible. It is important to realize that at places with strong damping of the acoustic wave (the front part of the core) there is a large momentum transfer from the acoustic wave to the fluid. This causes a very significant initial pressure increase at the front end of the core (see Figs. 7–13). The relative decrease in pressure at the front end at later times is caused by the temperature increase with time, which strongly influences the viscosity and the damping coefficient. These effects are well captured by our theoretical model.

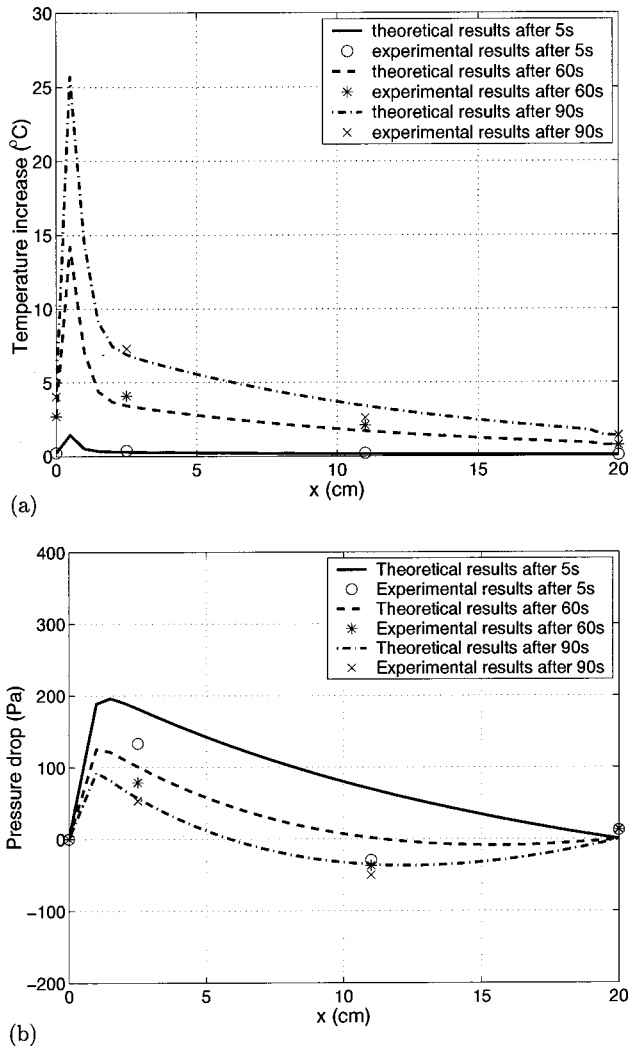


FIG. 7. Pressure and temperature profiles inside the core as functions of position plotted at three different times. Both experimental data and theoretical results are shown. The Berea sandstone core is saturated with 2% KCl brine. Frequency 20 kHz, permeability 270 mdarcy, $p_{\text{pore}}=120$ bars, $p_{\text{conf}}=185$ bars, and power input 250 W.

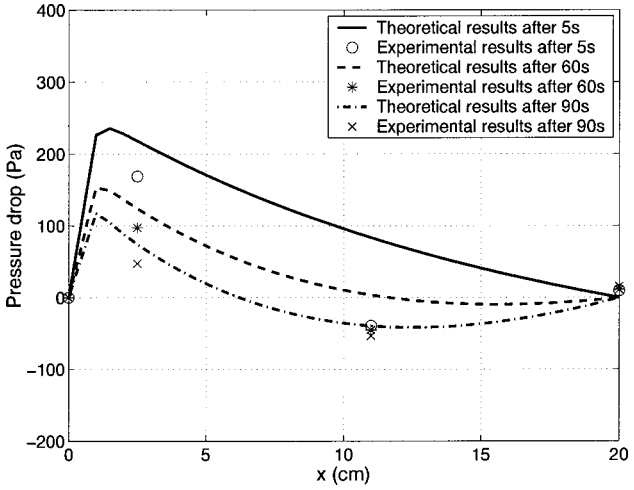


FIG. 8. Pressure profile inside the core as function of position plotted at three different times. Both experimental data and theoretical results are shown. The Berea sandstone core is saturated with 2% KCl brine. Frequency 20 kHz, permeability 270 mdarcy, $p_{\text{pore}} = 120$ bars, $p_{\text{conf}} = 185$ bars, and power input 300 W.

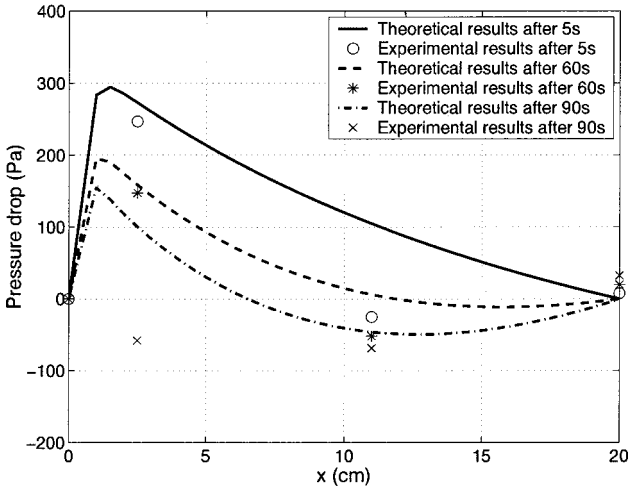


FIG. 10. Pressure profile inside the core as function of position plotted at three different times. Both experimental data and theoretical results are shown. The Berea sandstone core is saturated with 2% KCl brine. Frequency 20 kHz, permeability 270 mdarcy, $p_{\text{pore}} = 120$ bars, $p_{\text{conf}} = 185$ bars, and power input 375 W.

## VI. CONCLUSION

In this paper we have shown experimentally that a measurable acoustic streaming effect due to the dissipation of (high energy and high-frequency) acoustic waves can occur in a liquid inside a porous material. We measured the evolution of the pressure distribution in the liquid due to the momentum transfer from the acoustic waves to the liquid. Also the evolution of the temperature of the liquid due to the dissipation of acoustic energy was experimentally determined. The measurements were in reasonable agreement with model predictions based on an extension of the Darcy equation. Although the pressure changes due to acoustic streaming are measurable, it has to be kept in mind that the effect is rather weak. The pressure change due to acoustic streaming is much smaller than the pressure drop over the core resulting from a flow through the core at a typical (oil reservoir) flow rate of 75 ml/min. So during a practical application of high-frequency acoustic waves to clean the near well bore region of an oil reservoir the streaming effect is likely not relevant. However, from a scientific point of view the effect is very interesting.

## ACKNOWLEDGMENTS

We wish to thank Dr. D.M.J. Smeulders and De M.E.H. van Dongen for many discussions and suggestions they made to improve this work.

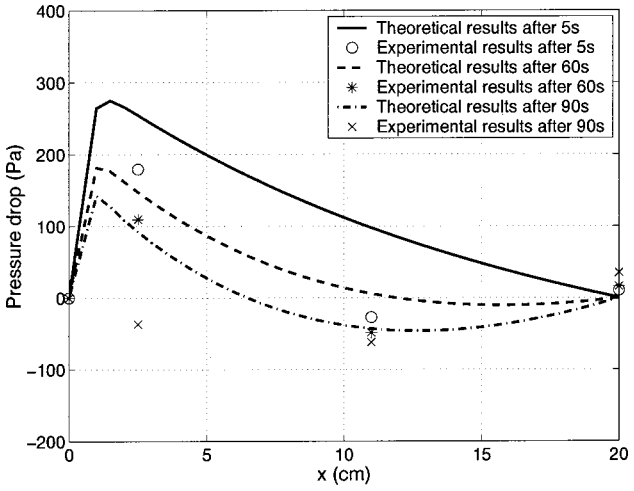


FIG. 9. Pressure profile inside the core as function of position plotted at three different times. Both experimental data and theoretical results are shown. The Berea sandstone core is saturated with 2% KCl brine. Frequency 20 kHz, permeability 270 mdarcy, $p_{\text{pore}} = 120$ bars, $p_{\text{conf}} = 185$ bars, and power input 350 W.

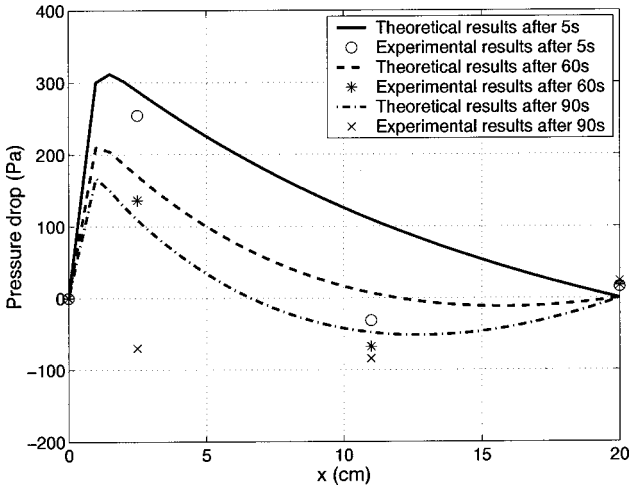


FIG. 11. Pressure profile inside the core as function of position plotted at three different times. Both experimental data and theoretical results are shown. The Berea sandstone core is saturated with 2% KCl brine. Frequency 20 kHz, permeability 270 mdarcy, $p_{\text{pore}} = 120$ bars, $p_{\text{conf}} = 185$ bars, and power input 400 W.

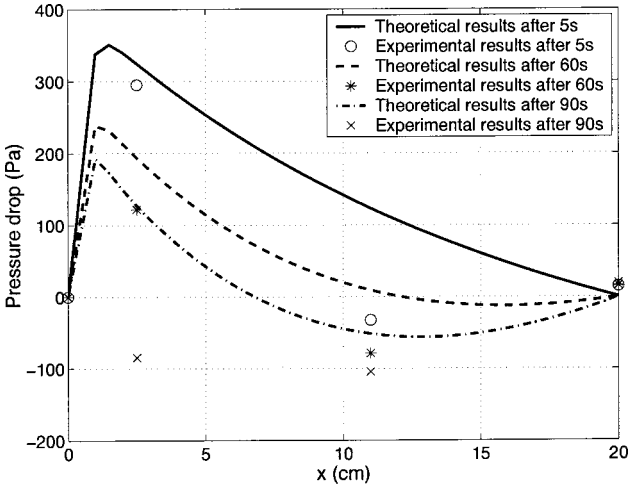


FIG. 12. Pressure profile inside the core as function of position plotted at three different times. Both experimental data and theoretical results are shown. The Berea sandstone core is saturated with 2% KCl brine. Frequency 20 kHz, permeability 270 mdarcy, $p_{\text{pore}} = 120$ bars, $p_{\text{conf}} = 185$ bars, and power input 450 W.

## APPENDIX A: BRIEF REVIEW OF BIOT'S THEORY AND THE CALCULATION OF DAMPING COEFFICIENT

Biot's theory allows one to calculate the velocity and the damping of acoustic elastic waves traveling through a porous material. In this appendix, we will give a brief review of this theory (simplified to the one-dimensional case). Introducing the averaged velocity of the solid, $w_s$, and the averaged velocity of the fluid, $w_f$ (the relation between $w_f$ and $v$ introduced in Sec. III is $v = \phi w_f$), the one-dimensional mass conservation laws for the solid and fluid phases in a porous medium can be written as

$$\frac{\partial}{\partial t}(1-\phi)\rho_s + \frac{\partial}{\partial x}(1-\phi)\rho_s w_s = 0, \tag{A1}$$

$$\frac{\partial}{\partial t}\phi\rho_f + \frac{\partial}{\partial x}\phi\rho_f w_f = 0, \tag{A2}$$

where $\phi$ is the porosity, and $\rho_f$ and $\rho_s$ are the densities of the fluid and solid, respectively. Linearization of Eqs. (A1) and (A2) yields

$$(1-\phi)\frac{\partial \rho_s}{\partial t} - \rho_s \frac{\partial \phi}{\partial t} + (1-\phi)\rho_s \frac{\partial w_s}{\partial t} = 0, \tag{A3}$$

$$\phi\frac{\partial \rho_f}{\partial t} + \rho_f \frac{\partial \phi}{\partial t} + \phi\rho_f \frac{\partial w_f}{\partial x} = 0. \tag{A4}$$

Assuming that the grains are incompressible, a combination of Eqs. (A3) and (A4) yields the so-called storage equation,

$$\frac{1}{K_f}\frac{\partial p}{\partial t} + \frac{1-\phi}{\phi}\frac{\partial w_s}{\partial x} + \frac{\partial w_f}{\partial x} = 0, \tag{A5}$$

where we used the constitutive relation for the pore fluid

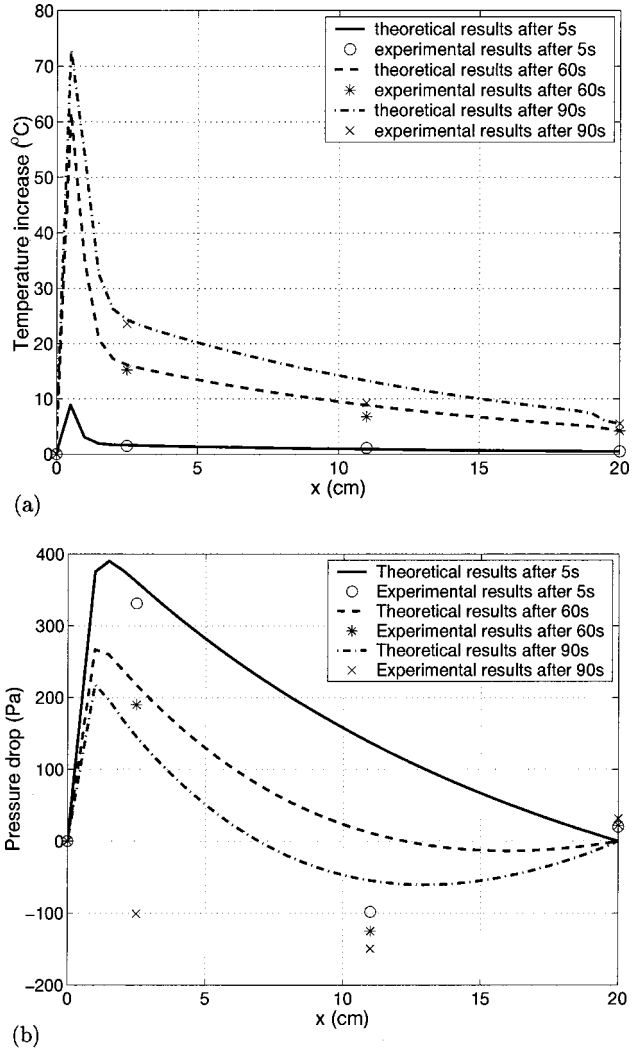


FIG. 13. Pressure and temperature profiles inside the core as function of position plotted at three different times. Both experimental data and theoretical results are shown. The Berea sandstone core is saturated with 2% KCl brine. Frequency 20 kHz, permeability 270 mdarcy, $p_{\text{pore}} = 120$ bars, $p_{\text{conf}} = 185$ bars, and power input 500 W.

$$\frac{1}{\rho_f}\frac{\partial \rho_f}{\partial t} = \frac{1}{K_f}\frac{\partial p}{\partial t}, \tag{A6}$$

where $K_f$ is the bulk modulus of the pore fluid.

The linearized momentum equations for the solid and the fluid are given by

$$(1-\phi)\rho_s \frac{\partial w_s}{\partial t} = -\frac{\partial \sigma}{\partial x} - (1-\phi)\frac{\partial p}{\partial x} - f_x, \tag{A7}$$

$$\phi\rho_f \frac{\partial w_f}{\partial t} = -\phi\frac{\partial p}{\partial x} + f_x, \tag{A8}$$

where we introduced the intergranular stress $\sigma$ (negative in tension), and the interaction force $f_x$ between the solid and the fluid phases. A detailed expression for $f_x$ will be given

later. We finally close the system of equations by means of Hooke's law, relating the stress and the strain in the solid material

$$\frac{\partial \sigma}{\partial t} = -K_p \frac{\partial w_s}{\partial x}, \tag{A9}$$

where $K_p$ is the constrained modulus (defined as $\lambda + 2\mu$, with $\lambda$ and $\mu$ the Lamé's coefficients). Taking Fourier's transform of Eqs. (A5)–(A9) with respect to both time and space and eliminating $p$ and $\sigma$, we obtain

$$-(1-\phi)\rho_s \omega^2 \hat{w}_s = -\left[K_p + K_f \frac{(1-\phi)^2}{\phi}\right]\hat{w}_s k^2 - (1-\phi)K_f \hat{w}_f k^2 - i\omega \hat{f}_x, \tag{A10}$$

$$-\phi \rho_f \omega^2 \hat{w}_f = -(1-\phi)K_f \hat{w}_s k^2 - \phi K_f k^2 \hat{w}_f + i\omega \hat{f}_x. \tag{A11}$$

At this stage it is necessary to provide an explicit formulation for $\hat{f}_x$. We have a precise definition due to the work of Johnson, Koplik, and Dashen [9]

$$\hat{f}_x = b(\omega)(\hat{w}_s - \hat{w}_f) + (\alpha_\infty - 1)\phi \rho_f i\omega(\hat{w}_s - \hat{w}_f), \tag{A12}$$

where we have introduced the tortuosity $\alpha_\infty$. The frequency dependent friction force $b(\omega)$ is expressed as

$$\frac{b(\omega)}{b_0} = \sqrt{1 + \frac{1}{2} iM \frac{\omega}{\omega_c}}, \tag{A13}$$

with $b_0 = \mu\phi^2/K_0$. $K_0$ is the stationary permeability, $M$ is the so-called similarity parameter, and $\omega_c$ is the critical frequency ($\omega_c = \mu\phi/K_0\rho_f\alpha_\infty$). Now solving Eqs. (A11) and (A12) we arrive at the dispersion relation

$$d_2 \psi^2 + d_1 \psi + d_0 = 0, \tag{A14}$$

in which different quantities are defined by

$$d_2 = PR - Q^2,$$

$$d_1 = -(P\rho_{22} + R\rho_{11} - 2Q\rho_{11} - 2Q\rho_{12}) + \frac{ib(\omega)}{\omega}(P + R + 2Q),$$

$$d_0 = \rho_{11}\rho_{22} - \rho_{12}^2 \frac{ib(\omega)}{\omega},$$

$$P = K_p + K_f \frac{(1-\phi)^2}{\phi},$$

$$Q = (1-\phi)K_f, \tag{A15}$$

$$R = \phi K_f,$$

$$\rho_{12} = -(\alpha_\infty - 1)\phi \rho_f,$$

$$\rho_{11} = (1-\phi)\rho_s - \rho_{12},$$

$$\rho_{22} = \phi \rho_f - \rho_{12},$$

$$\psi = \left(\frac{k}{\omega}\right)^{1/2}.$$

Since the frequency is known, from Eq. (A14) we can calculate the wave number ($k$) and then the velocity and the damping coefficient of the two waves. For instance, using the parameters given in Table I we derive the wave velocities and damping coefficients given in Table II.

TABLE I. Parameters used for the calculation of the wave properties.

| Parameter | Value |
|---|---|
| Permeability | $0.1974 \times 10^{-12}$ m$^2$ |
| Porosity | 25% |
| $K_p$ | 36.1 GPa |
| $K_f$ | 2.06 GPa |
| $\mu$ | $9.8 \times 10^{-4}$ (Pa s) |
| $\rho_f$ | 1000 kg/m$^3$ |
| $\rho_s$ | 2640 kg/m$^3$ |
| $\omega$ | 40 kHz |
| $\alpha_\infty$ | 2.8 |
| $M$ | 1 |

## APPENDIX B: CALCULATION OF TRANSMITTED FAST AND SLOW WAVES ACCORDING TO WU, XUE, AND ADLER [7]

Wu, Xue, and Adler [7] developed a calculation procedure to deal with the problem of the transmission and reflection of acoustic waves at the interface between a fluid and a porous material. The transmitted and reflected intensities are calculated by using the Poynting energy flux vector. We simplify the problem to the case of waves propagating perpendicular to the interface; in that case the shear wave is absent. If we introduce the potentials $\phi_+$ and $\phi_-$ of the fast and slow wave (we will use the subscript + and − pointing, respectively, to fast and slow wave properties), we can write the displacements (for the free fluid, $U'$, the fluid in the porous medium, $U$, and the solid material, $u$) as

$$U' = \frac{d\phi_f}{dx}, \tag{B1}$$

TABLE II. Wave velocities and damping coefficient.

| Parameter | Value |
|---|---|
| $c_{\text{fast}}$ | 4833.6 m/s |
| $c_{\text{slow}}$ | 658.4 m/s |
| $\alpha_{\text{fast}}$ | 0.28 m$^{-1}$ |
| $\alpha_{\text{slow}}$ | 182.3 m$^{-1}$ |

$$u=\frac{d\phi_+}{dx}+\frac{d\phi_-}{dx}, \tag{B2}$$

$$U=-G_+\frac{d\phi_+}{dx}-G_-\frac{d\phi_-}{dx}, \tag{B3}$$

where the coefficients $G_{+,-}$ are given by

$$G_{+,-}=\frac{c_{+,-}^2\rho_{11}-P}{c_{+,-}^2\rho_{12}-Q}, \tag{B4}$$

where $c_{+,-}$ are the velocities of the fast and slow waves. We can now impose the following three boundary conditions valid for the case of an open pore boundary condition.

(1) Continuity of normal stress,

$$(P+Q)\frac{du}{dx}+(Q+R)\frac{dU}{dx}-K_f\frac{dU'}{dz}=0. \tag{B5}$$

(2) Conservation of fluid volume,

$$\phi U+(1-\phi)u=U'. \tag{B6}$$

(3) Proportionality between discontinuity in pressure and relative velocities in porous medium,

$$(1/\phi)\left[Q\frac{du}{dx}+R\frac{dU}{dx}\right]-K_f\frac{dU'}{dx}=0. \tag{B7}$$

We define the Poynting vector as

$$\mathbf{P}=-\dot{\mathbf{u}}\cdot\mathbf{T}-\dot{\mathbf{U}}S, \tag{B8}$$

where $\mathbf{T}$ is the stress tensor in the skeleton and $S$ is the strain tensor. In one-dimensional case problem (assuming $z$ the direction of propagation), the Poynting vector can be simplified as

$$\mathbf{P}=-i\omega[\mathbf{i}_z(uT+US)]. \tag{B9}$$

The displacement potential can now be written as

$$\begin{aligned}\phi_f&=(e^{-i\gamma_f x}+Ae^{i\gamma_f x})e^{-i\omega t},\\ \phi_+&=B_+e^{-i\gamma_+ x}e^{-i\omega t},\\ \phi_-&=B_-e^{-i\gamma_- x}e^{-i\omega t},\end{aligned} \tag{B10}$$

where the amplitude of the incident wave is taken equal to unity. $A$ is the amplitude of the reflected wave and $B_+$ and $B_-$ are the amplitudes of the transmitted waves. In addition we have

$$\begin{aligned}\gamma_f^2&=\omega^2/V_f^2,\\ V_f&=(K_f/\rho_f)^{1/2},\\ \gamma_+&=\omega/c_+,\\ \gamma_-&=\omega/c_-.\end{aligned} \tag{B11}$$

If we now substitute the Eqs. (B1)–(B4) and (B10) and (B11) in Eqs. (B5)–(B7), we can determine $A$, $B_+$, and $B_-$ and then the displacements. For fast and slow waves, we derive the following result:

$$\begin{aligned}u&=-i\gamma_+\phi_+-i\gamma_-\phi_-,\\ U&=-i\gamma_+G_+\phi_+-i\gamma_-G_-\phi_-,\\ T&=[(QG_+-P+2N)\omega^2/c_+^2-2N\gamma_+^2]\phi_+\\ &\quad+[(QG_--P+2N)\omega^2/c_-^2-2N\gamma_-^2]\phi_-,\\ S&=(RG_+-Q)\omega^2/c_+^2\phi_++(RG_--Q)\omega^2/c_-^2\phi_-.\end{aligned} \tag{B12}$$

If we substitute Eqs. (B12) in Eq. (B9) and take the absolute value of the Poynting vector, we obtain the sound intensity of the fast and slow waves in the fluid-saturated porous media,

$$\begin{aligned}I_+&=[(-2Q+RG_+)G_++P]\omega^4/c_+^3|\phi_+|^2,\\ I_-&=[(-2Q+RG_-)G_-+P]\omega^4/c_-^3|\phi_-|^2.\end{aligned} \tag{B13}$$


[1] P. Poesio, G. Ooms, S. Barake, and F. v. Bas, J. Acoust. Soc. Am. **111**, 2019 (2002).

[2] S. Barake, F. v. Bas, G. Ooms, and P. Poesio (unpublished).

[3] J. Lighthill, *Waves in Fluids* (Cambridge University Press, Cambridge, 1978).

[4] K. C. Khilar and H. S. Fogler, *Migration of Fines in Porous Media* (Kluwer Academic, Dordrecht, 1998), pp. 23-53.

[5] S. Zaytsev and V. Aseyev, *Properties of Aqueous Solution of electrolytes* (CRC, Boca Raton, FL, 1992), pp. 216-218.

[6] M. A. Biot, J. Acoust. Soc. Am. **28**, 168 (1956).

[7] K. Wu, Q. Xue, and L. Adler, J. Acoust. Soc. Am. **87**, 2349 (1990).

[8] A. M. Khan and I. Fatt, Soc. Pet. Eng. J. **5**, 113 (1965).

[9] D. L. Johnson, J. Koplik, and R. Dashen, J. Fluid Mech. **176**, 379 (1987).